COBEM 2023 27TH INTERNATIONAL CONGRESS OF MECHANICAL ENGINEERING

ABCM Brazilian Society of Mechanical Sciences and Engineering
27th ABCM International Congress of Mechanical Engineering
December 04-08, 2023, Florianópolis-SC, Brazil

COB-2023-0613
IMPACT OF AIRFOIL THICKNESS ON THE ROTATIONAL EFFECT OVER WIND-TURBINE-BLADE FLOW

Daniel Sampaio Souza
Nathan Oliveira Assis
School of Engineering, São Paulo State University (UNESP), Campus São João da Boa Vista, São João da Boa Vista 13876-750, Brazil
daniel.s.souza@unesp.br
nathan.oliveira@unesp.br

Abstract. *The aerodynamic load on inboard sections of rotating wings is often significantly greater than the one expected for the corresponding airfoil at rectilinear motion with the same angle of attack and Reynolds number. A better understanding of this phenomenon, frequently referred to as rotational augmentation, is of great importance for the development of more reliable aerodynamic prediction tools. The aim of this research is to investigate the impact of airfoil thickness on the response to the blade-section rotation of the flow and of the aerodynamic performance considering conditions representative of horizontal-axis wind turbines. Reynolds-averaged Navier-Stokes simulations in a non-inertial reference frame considering periodicity in the spanwise direction were carried out using the open-source package OpenFOAM. The results indicate that the effect of rotation on drag depends on the airfoil thickness. Moreover, they corroborate that a mechanism different from the centrifugal pumping, probably the radial planetary vorticity tilting, is relevant for the volume reduction caused by rotation on the region of separated flow. For both geometries at the tested conditions, the results suggest that the rotational lift increase is due to the weakening of the decambering effect which, in turn, is a consequence of the aforementioned volume reduction.*

Keywords: *HAWT, rotational augmentation, finite-volume method.*

1. INTRODUCTION

The aerodynamic behavior of inboard sections of rotating wings frequently differs from the behavior of the corresponding airfoil section in rectilinear motion. It is known that rotation increases the sectional lift (Harris, 1966) what is known as rotational augmentation. Several engineering models were proposed to take the phenomenon into account within the framework of horizontal-axis-wind-turbine (HAWT) blade-design tools. However, the variability of the models (Breton *et al.*, 2007) reveals the lack of understanding about the phenomenon.

The rotational augmentation is sometimes attributed to a delay of the boundary layer separation. The streamwise component of the Coriolis force provides momentum to the boundary layer, improving the resistance to separation (Du and Selig, 2000).

Another plausible mechanism relevant to the rotational augmentation is the centrifugal pumping (Lindenburg, 2003). Since the centrifugal force scales with r, the distance to the rotor axis, there is a radial gradient of this force that pumps the vortical flow from inboard sections towards the blade tip, reducing the thickness of the viscous layer over the airfoil and thus weakening the decambering effect (Bangga *et al.*, 2017). Souza and Gennaro (2020) conducted spanwise-periodic, Reynolds-averaged Navier-Stokes (RANS) simulations considering the effect of Coriolis and centrifugal forces at angles of attack of 12 deg and 16 deg. The model neglected the spanwise variation of the centrifugal force and the simulations did not capture any significant spanwise variation of the flow-field variables. However, Souza and Gennaro (2020)'s results predicted a substantial volume reduction of the region of separated flow close to the airfoil trailing edge. Suggesting that another rotation-related mechanism may play a role in the section load enhancement.

An excess lift is observed in insect wings due to the stabilization of the leading-edge vortex (LEV) (Eldredge and Jones, 2019). Among the mechanisms underlying the LEV-stabilization is the radial planetary vorticity tilting (Werner *et al.*, 2019), which is the contribution of the streamwise component of the Coriolis acceleration to the spanwise-vorticity equation. In the context of HAWT's inboard blade sections, Rodrigues *et al.* (2019) have shown that this mechanism is relevant for the balance of spanwise vorticity in the separated flow on the blade suction surface.

Regarding the sectional drag, the effect of rotation is ambiguous. Three-dimensional RANS simulations by Herráez *et al.* (2014) have identified drag reduction at some portions and drag increase in other portions of the same blade. Since different profile geometries were employed in the blade, they argued that the rotational effect on drag may be geometry dependent. Results by Souza and Gennaro (2020) and Rodrigues *et al.* (2019) indicates that it depends also on the angle of attack.

The aim of the work described here is to investigate the influence of airfoil thickness on the rotational effects. The

same RANS model used by Souza and Gennaro (2020) was employed to simulate the flow over two airfoils with different thicknesses at 12 deg angle of attack. The focus is on the effect of rotation on the drag and on the region of separated flow close to the airfoil trailing edge.

2. METHODOLOGY

2.1 Airfoil geometries

This study considered two airfoil geometries, the baseline S809 airfoil, designed by Somers (1997) for application in wind turbine blades, and a modified, thinner S809 profile, hereafter named as S809mod. The modified airfoil had an thickness equal to 16% of the chord, in contrast to the 21% thickness of the original geometry. To perform this modification the open-source software XFLR5 was used so that the airfoil's camber distribution and maximum thickness location were preserved. Figure 1 compares the profile of both airfoils.

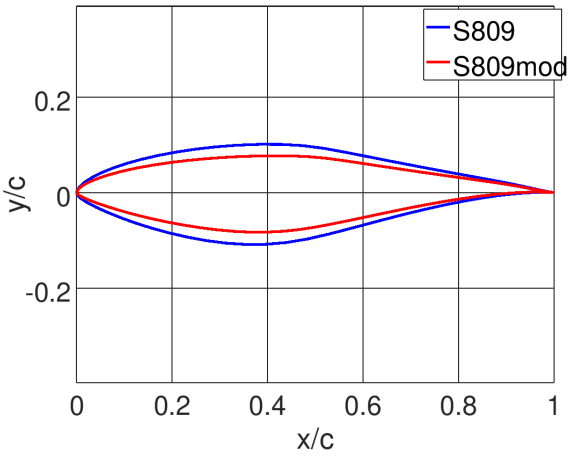

Figure 1. Geometry of the simulated airfoils.

2.2 Computational model

The simulations were performed using the open-source package OpenFOAM. The same steady RANS model employed by Souza and Gennaro (2020) was used for the study described here. Since for typical operational conditions of HAWT blades inboard sections the speed is significantly lower than the sound speed, the flow was assumed incompressible and a representative Reynolds number of 1×10^6 was considered.

For each airfoil two conditions were considered, one without the effect of rotation and one in which the Coriolis and centrifugal accelerations were considered. To account for these non-inertial effects, additional terms were included in the momentum equation (Souza and Gennaro, 2020). The rotational condition was adjusted according to the Rossby number, $Ro = U_\infty \Omega^{-1} c^{-1}$, where U_∞ is the freestream velocity, Ω is the angular velocity and c is the airfoil chord. For the condition with rotation, an Rossby number of 3 was considered. Another non-dimensional parameter determining the blade-section flow's dynamic is the local velocity ratio, $\Lambda = U_\infty \Omega^{-1} r^{-1}$, where r is the distance between the section and the rotor axis. A unity local velocity ratio was considered for the rotational condition.

The domain size and computational mesh was chosen based on the convergence study performed by Souza and Gennaro (2020). Figure 2 shows planar views of the employed domain and the grid used for the modified geometry. The domain extends 20 chords upstream, over and below the airfoil leading edge and 30 chords downstream. In the spanwise direction the domain had an extension of three chords and periodicity was considered. However, identically to the results by Souza and Gennaro (2020), in the present results there was no observable variation of the flow field in this direction.

A multi-block C-shaped grid was employed. The airfoil was discretized through 41 elements, the wake 153 divisions were employed to the wake and 123 to the airfoil-normal direction, with a refinement set-up in the boundary-layer region sufficient to keep the y^+ of the first cell layer over the airfoil below 3. In the spanwise direction the domain was divided in 30 equally refined divisions.

Dirichlet boundary condition was imposed for the velocity on the inlet and for the pressure on the outlet, while Neumann boundary condition was imposed to the pressure on the inlet and the velocity on the domain outlet. On the top and bottom domain boundary, inviscid wall condition was considered. Velocity-pressure coupling was performed by the SIMPLE algorithm was run until the residuals of velocity and pressure decayed at least three orders of magnitude. An

exception for this convergency criterion was adopted for the spanwise velocity component in the cases without rotation. Since its values was nominally zero throughout the domain in these cases, its residuals could not converge to the prescribed level. The cases were run in parallel using 6 processes through MPI protocols as implemented in OpenFOAM libraries. For further details about the simulation model, the reader should refer to Souza and Gennaro (2020).

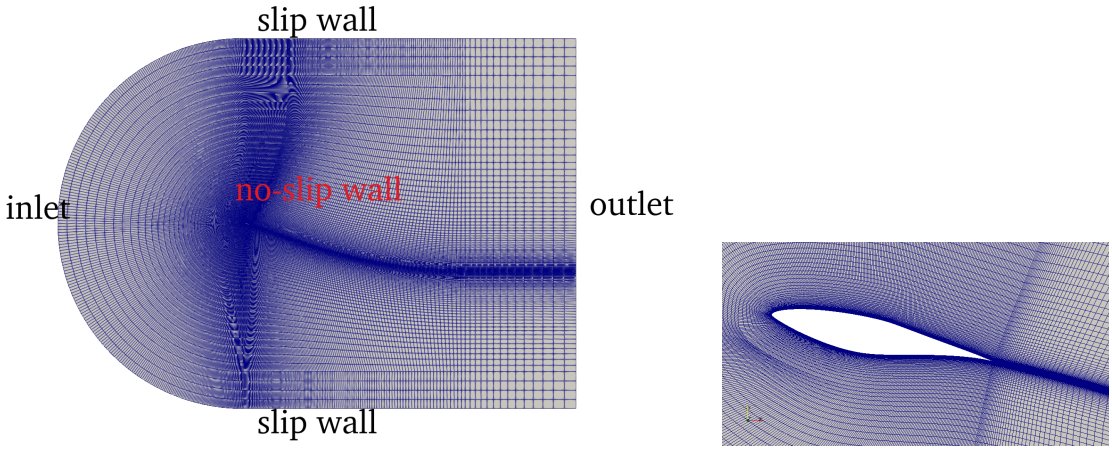

(a) (b)

Figure 2. (a) Sectional view of the computational domain and grid and (b) detailed view of the grid in the airfoil region for the modified airfoil.

3. RESULTS

Table 1 depicts the lift coefficient predicted for the simulated cases. The table also shows the contribution of the pressure and shear stress for the coefficient. The expected lift increase due to rotation was clearly observed for both geometries. It is seen that this effect was more intense on the original S809 geometry, for which an increase of 31% was observed. Moreover, the relative contribution of the surface tensions to the lift did not change with rotation and the pressure was almost the sole contribution for this force component for all cases.

Table 1. Lift coefficient (C_l) and the contribution of pressure $C_{l,p}$ and wall shear stress $C_{l,\tau}$.

	$Ro = \infty$			Ro=3			
airfoil	C_l	$C_{l,p}$	$C_{l,\tau}\times10^4$	C_l	variation [%]	$C_{l,p}$	$C_{l,\tau}\times10^4$
S809	0.99887	0.99853	3.5383	1.3104	31.2%	1.3099	5.0453
S809mod	1.0055	1.0053	1.3679	1.2313	22.5%	1.2311	1.4847

The predicted drag and the contributions from pressure and wall shear stress is shown in Tab. 2. Interestingly, the effect of rotation on the drag was not so obvious as on the lift. For the baseline airfoil, the drag reduced as rotation was introduced, while for the modified geometry the drag increased. As shown by Assis and Souza (2023), for these two geometries, this opposing response also occurs for rotation at higher Rossby numbers. This observation is in agreement with Herráez *et al.* (2014), who claim that the rotational effect on drag depends on the airfoil geometry.

Table 2. Drag coefficient (C_d) and the contribution of pressure $C_{d,p}$ and wall shear stress $C_{d,\tau}$.

	$Ro = \infty$			Ro=3			
airfoil	C_d	$C_{d,p}$	$C_{d,\tau}$	C_d	variation [%]	$C_{d,p}$	$C_{d,\tau}$
S809	0.049221	0.043233	0.0059877	0.047604	-3.3%	0.041509	0.0060949
S809mod	0.056629	0.052653	0.0041765	0.065857	16.3%	0.062088	0.0037685

It is important to note that other results indicate that it depends also on the angle of attack (Souza and Gennaro, 2020; Rodrigues *et al.*, 2019). In Souza and Gennaro (2020) and Rodrigues *et al.* (2019), it is argued that the matter is dictated by the orientation towards which the increased suction on the airfoil upper surface acts predominantly. Increased suction on the airfoil aft portion contributes to increase the drag while suction on the fore portion tends to reduce the drag. Since

both the angle of attack and airfoil thickness determine the portions of the suction side facing against and towards the freestream, these two characteristics influence the effect of rotation on the drag. This hypothesis is in line with the data in Tab. 2, which shows that the drag increase for the S809mod airfoil is due to the pressure contribution. In fact, for S809mod, the frictional drag reduced with rotation.

Figure 3 shows the pressure coefficient (C_p) distribution over the central section of computational domain. The vertical lines indicate the location of the separation point. For both geometries, it was observed that the rotation enhanced the suction over the entire airfoil's upper surface. Moreover, it is seen that the suction peaks strengthened significantly, particularly for the S809mod airfoil. Regarding the separation point, it is seen that as the thickness was reduced the separation moved downstream, both with and without rotation. This seems to be associated to the fact that the baseline airfoil had an pronounced pressure gradient around x/c=0.5 that does not occur for the modified geometry. Probably due the same reason, the rotation delayed the separation further for the modified airfoil in comparison to the original one.

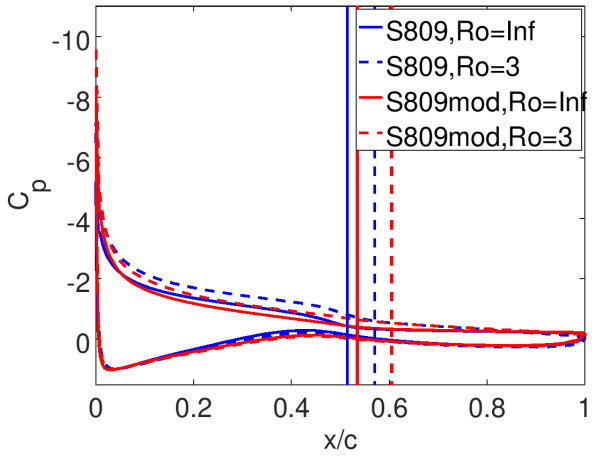

Figure 3. Distribution of pressure coefficient (C_p) over the airfoils' surface predicted by the simulations. Vertical lines denote the separation point.

The dividing streamline along with the rotation center of the recirculating flow is shown in Fig. 4 for the central section of the computational domain. For both airfoils, it is seen that the region of recirculating flow reduced significantly with rotation. Note that, for the S809mod airfoil at the condition with Ro=3, the rotation center could not be identified. This reduction of the region of separated flow was also observed by Souza and Gennaro (2020) for the S809 geometry at angles of attack equal 12 deg and 16 deg and is consistent with the flow over inboard sections of HAWT blades (Bangga *et al.*, 2017). However, as discussed in Souza and Gennaro (2020), the volume reduction of the recirculating region cannot be attributed to the centrifugal pumping, since the simulation model employed here does not account for the radial variation of the centrifugal force and the simulations did not present appreciable spanwise variations of the flow field. An alternative explanation for such variation is the destruction of spanwise vorticity by the effect of the streamwise component of the Coriolis force, the so-called radial planetary vorticity tilting (Werner *et al.*, 2019; Eldredge and Jones, 2019), which, may have a relevant contribution for the balance of spanwise vorticity in the region of separated flow (Rodrigues *et al.*, 2019).

For conditions typical of insect flight, the aforementioned planetary vorticity tilting contributes to stabilize the leading-edge vortex on the wing's upper surface, which in turn remains attached providing additional lift (Wojcik and Buchholtz, 2014; Jardin, 2017; Werner *et al.*, 2019; Eldredge and Jones, 2019). We investigated the circulation around the region of separated flow for both airfoils and how it is affected by rotation. With this aim, a region representative of the recirculating flow was chosen for each simulated case. Figure 5 highlight the selected regions in black underneath the streamlines. The circulation attributed to the region of recirculating flow Γ was computed as

$$\Gamma = \iint_{\Sigma} \omega_z dS, \tag{1}$$

where Σ denotes the selected region and ω_z the spanwise vorticity component.

From the circulation given by Eq. 1, the ratio between a vortex lift coefficient, computed through the Kutta-Joukowski theorem, and the airfoil lift coefficient was calculated and is given in Tab. 3. We observe that without rotation, the vortex lift is over half of the total airfoil lift. However, for the rotational condition considered, the vortex-to-airfoil lift ratio reduces substantially. This result indicates that, for the conditions tested here, the lift increase caused by rotation is not

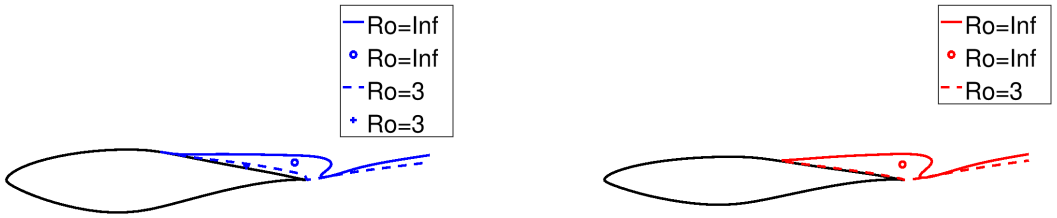

(a) S809 (b) S809mod

Figure 4. Central section dividing streamline on the upper surface of the the airfoils. Symbols indicate the rotation center of the recirculating flow, which could not be identified for S809mod airfoil in rotational condition.

associated with the mechanism observed in insects, i.e., the stabilization of a lift-contributing vortex. The viscous layer over the airfoil surface and, most notably, the separation of the boundary layer close to the trailing edge, reduces the effective airfoil camber and, by reducing the height of the region of separated flow, the rotation reduces the impact of this effect. As already pointed out by Bangga *et al.* (2017), this weakening of the decambering effect seems to be the mechanism underlying the lift increase due to rotation at the conditions considered here.

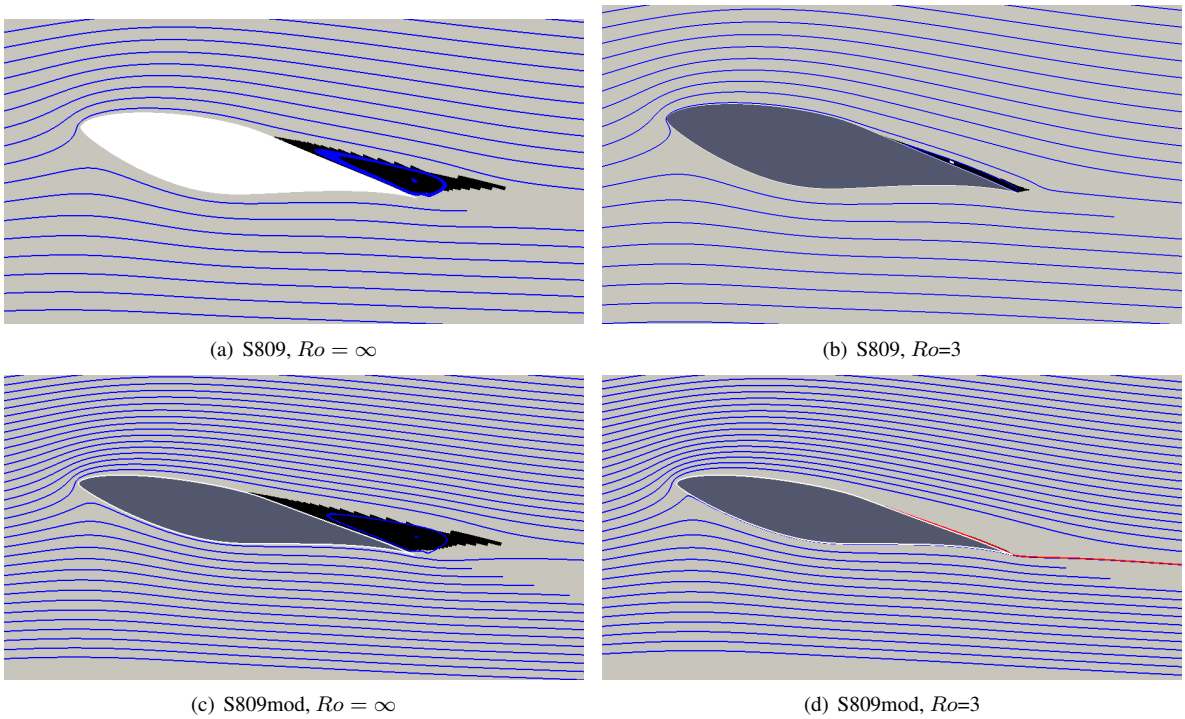

(a) S809, $Ro = \infty$ (b) S809, Ro=3

(c) S809mod, $Ro = \infty$ (d) S809mod, Ro=3

Figure 5. Sectional streamlines on the central section of the domain superimposed on the integration region considered for evaluation of Eq. 1.

Table 3. Ratio between vortex lift coefficient and the airfoil lift coefficient.

airfoil	$Ro = \infty$	Ro=3
S809	65.9%	5.76%
S809mod	54.6%	2.67%

4. CONCLUSION

Numerical simulations of RANS type was carried to investigate the influence of airfoil thickness on the rotational effect on horizontal-axis wind-turbine section flow at 12 deg angle of attack. Two airfoil geometries were considered and, for each geometry, one condition considering rotation was simulated besides the condition at rectilinear motion. The rotational augmentation, i.e. the lift increase with rotation, was observed for both geometries. However, the effect of rotation on the drag differed for the tested geometries: for the thicker airfoil, the rotation reduced the drag, while for the thinner one, the drag increased as the effect of rotation was introduced. It is important to note that the drag increase for the latter was solely due to the pressure contribution, since the frictional drag reduced with rotation. Although the simulations did not capture spanwise variations of the flow field, they predicted a reduction of the volume of the region of separated flow close to the airfoil trailing edge due to rotation for both geometries. This might be a consequence of the destruction of spanwise vorticity by the gradient of the streamwise Coriolis acceleration, which is responsible for lift increment on insect wings through the stabilization of the leading-edge vortex. However, according to the present results - considering conditions representative of inboard sections of HAWT blades - the rotation reduces substantially the circulation of the recirculating flow. Therefore, our results suggest that, for the tested conditions, rather than vortex stabilization, the lift increase is attributed to the weakening of the decambering effect.

5. ACKNOWLEDGEMENTS

N. Assis acknowledges financial support by Associação Brasileira de Engenharia e Ciências Mecânicas (ABCM).

6. REFERENCES

Assis, N. and Souza, D., 2023. "Estudo do efeito da espessura do aerofólio sobre o aumento rotacional em seções de pás de turbina eólica". In *Anais do XXIX Congresso Nacional de Estudantes de Engenharia Mecânica*. Goiânia, Brazil.

Bangga, G., Lutz, T., Jost, E. and Krämer, E., 2017. "CFD studies on rotational augmentation at the inboard sections of a 10MW wind turbine rotor". *Journal of Renewable and Sustainable Energy*, Vol. 9, pp. 1–28.

Breton, S., Coton, F. and Moe, G., 2007. "A study on rotational effect and different stall delay models using a prescribed wake vortex scheme and NREL phase VI experiment data". *Wind Energy*, Vol. 11, pp. 459–482.

Du, Z. and Selig, M., 2000. "The effect of rotation on the boundary layer of a wind turbine". *Renewable Energy*, Vol. 20, pp. 167–181.

Eldredge, J.D. and Jones, A.R., 2019. "Leading-edge vortices: Mechanics and modeling". *Annual Review of Fluid Mechanics*, Vol. 51, pp. 75–104.

Harris, F., 1966. "Preliminary study of radial flow effects on rotor blades". *Journal of American Helicopter Society*, Vol. 11, No. 3, pp. 1–21.

Herráez, I., Stoevesandt, B. and Peinke, J., 2014. "Insight into rotational effects on a wind turbine blade using Navier-Stokes computations". *Energies*, Vol. 7, pp. 6798–6822.

Jardin, T., 2017. "Coriolis effect and the attachment of the leading edge vortex". *Journal of Fluid Mechanics*, Vol. 820, pp. 312–340.

Lindenburg, C., 2003. "Investigation into rotor blade aerodynamics". Technical report, NOVEM, Netherlands.

Rodrigues, P.T., Gennaro, E.M. and Souza, D.S., 2019. "Effect of coriolis acceleration on the span-wise vorticity field over a wind-turbine airfoil". In *AIAA AVIATION 2022 Forum*. Chicago, USA.

Somers, D.M., 1997. "Design and experimental resultos for the S809 airfoil". Technical report, NREL.

Souza, D. and Gennaro, E., 2020. "Rotational effects on the spanwise periodic flow over a wind turbine airfoil". In *Proceedings of 18th Brazilian Congress of Thermal Sciences and Engineering*. Online.

Werner, N., Chung, H., Wang, J., Liu, G., Cimbala, J., Dong, H. and Cheng, B., 2019. "Radial planetary vorticity tilting in the leading-edge vortex of revolving wings". *Physics of Fluids*, Vol. 31, pp. 1–15.

Wojcik, C. and Buchholtz, J., 2014. "Vorticity transport in the leading-edge vortex on a rotating blade". *Journal of Fluid Mechanics*, Vol. 743, pp. 249–261.

7. RESPONSIBILITY NOTICE

The authors are solely responsible for the printed material included in this paper.